Polymer Chemistry

ROYAL SOCIETY OF CHEMISTRY

PAPER

View Article Online
View Journal | View Issue

Cite this: *Polym. Chem.*, 2026, **17**, 1100

Effect of 4-vinylpyridine incorporation on the shape transformation of poly(ethylene glycol)-*block*-polystyrene polymersomes

Işıl Yeşil Gür, [a] Duru Ulukan,[b] Jingxin Shao, [a] Yiğitcan Sümbelli, [a] Alexander B. Cook, [a] Johan P. A. Heuts, [c] Jan C. M. van Hest *[a] and Loai K. E. A. Abdelmohsen *[a]

The self-assembly of block copolymers enables the formation of diverse nanostructures, among which polymeric vesicles (polymersomes) are particularly significant. Poly(ethylene glycol)-*block*-polystyrene (PEG-PS) copolymers are known to self-assemble into polymersomes that can further undergo a shape transformation into bowl-shaped stomatocytes, a morphology that has been extensively studied. In this work, we investigated the incorporation of 4-vinylpyridine (4VP) into the hydrophobic domain of PEG-PS copolymers to introduce membrane functionality and broaden stomatocyte applications. We systematically examined the influence of 4VP content and polymer architecture on stomatocyte formation. The stomatocyte morphology was characterized qualitatively by electron microscopy and quantitatively by asymmetric flow field-flow fractionation (AF4) coupled with multi-angle light scattering (MALS) and quasi-elastic light scattering (QELS) detectors (AF4-MALS-QELS) using the shape factor (R_g/R_h). Our findings reveal that the presence of 4VP significantly affected stomatocyte formation, leading to reduced stomatocyte populations compared to that with the PEG-PS system. This required thorough optimization of both the polymer composition and shape transformation conditions to achieve optimal stomatocyte formation, demonstrating that even subtle variations in the hydrophobic domain can profoundly influence the resulting morphology. The presence of 4VP in the stomatocytes brought additional functionality and made it possible to coordinate copper, which was shown to be effective in the model CuAAC reaction.

Received 8th December 2025,
Accepted 11th February 2026

DOI: 10.1039/d5py01163a

rsc.li/polymers

1. Introduction

Block copolymers have been the focus of extensive research over the past decades because of their remarkable versatility and applicability as building blocks for a wide variety of self-assembled materials.[1–3] Their ability to undergo phase separation – either in bulk or in selective solvents – results in the formation of ordered nanostructures with diverse morphologies, such as spheres, tubes, lamellae, and vesicles.[4–6] These assemblies can be used as stabilizers in emulsion polymerization,[7,8] lubricant additives,[9] and carriers in drug and gene delivery systems.[10–12]

In recent decades, the factors contributing to the self-assembly of block copolymers have been extensively studied.[5,13–16] For diblock copolymers composed of monomers A and B, the interactions between A–A, B–B and A–B play a significant role in their phase separation and consequent self-assembly.[6] The ratio between the hydrophilic and hydrophobic fractions and their chemical nature are important parameters that directly impact the resulting morphologies,[15] and additionally the polymer concentration influences aggregation behaviour.[17] In solution, the self-assembly of block copolymers is furthermore dependent on the interactions between the polymer building blocks and the solvent.[14,18,19] The assembly method also plays an important role in determining what type of particles can be obtained.[20]

By changing the conditions, diverse morphologies are attained through block copolymer self-assembly. One interesting structure is the polymeric vesicle, often termed a polymersome; it stands out due to its unique structural features and robust properties. Comprising a bilayered hydrophobic membrane surrounding an aqueous lumen, polymersomes exhibit greater stability and mechanical strength compared to their lipid-based counterparts.[21] In addition, spherical polymer-

[a]*Bio-Organic Chemistry, Department of Chemical Engineering & Chemistry, Institute for Complex Molecular Systems (ICMS), Eindhoven University of Technology, 5600 MB Eindhoven, The Netherlands. E-mail: j.c.m.v.hest@tue.nl, l.k.e.a.abdelmohsen@tue.nl*
[b]*Department of Chemistry, Boğaziçi University, Bebek, Istanbul 34342, Turkey*
[c]*Supramolecular Polymer Chemistry, Department of Chemical Engineering & Chemistry, Institute for Complex Molecular Systems (ICMS), Eindhoven University of Technology, 5600 MB Eindhoven, The Netherlands*

somes, the thermodynamically stable topology, are prone to shape transformation into a range of kinetically trapped structures, amongst which are the bowl-shaped morphologies named stomatocytes. Besides traditional functionalisation strategies used for polymersomes, such as the surface display of active components,[22,23] stomatocytes offer additional opportunities *via* the extra internal cavity directly connected to the outside environment *via* a "neck" region. This enables the encapsulation of inorganic nanoparticles such as manganese dioxide[24] and cerium oxide,[25] enzymes such as urease,[23] catalase[26] or even multiple enzymes,[27,28] clearly demonstrating the stomatocytes' application potential.

Unlike the modification of the surface and the inner cavity, the chemical versatility of the stomatocyte membrane has been less explored. This is also less trivial, as the polymersome shape change process can be very sensitive to chemical adjustments of the building blocks. Even the introduction of an azide moiety at the end of the poly(ethylene glycol) (PEG) block changed the hydrodynamic volume of the hydrophilic part to such an extent that hexagonally packed hollow hoops were formed rather than stomatocytes under standard dialysis conditions.[29] Inspired by the recent literature based on poly (ethylene glycol)-*block*-polystyrene (PEG-PS) stomatocytes,[23,26,27,29–35] this paper focuses on membrane modification by incorporating 4-vinyl pyridine (4VP) into the stomatocyte bilayer. This is motivated by the fact that 4VP introduces additional functionality, such as the ability to chelate metal catalysts including copper,[36] palladium[37] and gold[38] and to operate as a polymer-supported catalyst.[39] For this specific reason, 4VP has already been incorporated into block copolymers and supramolecular systems.[40–44] Furthermore, 4VP incorporation introduces pH responsiveness into block copolymers[45] and can also be used to facilitate the formation of polymer–inorganic hybrid materials.[46,47]

To further expand the versatility of the stomatocyte platform, we aimed to introduce the chemical functionality directly into the vesicle membrane by incorporating 4-vinylpyridine (4VP) into the hydrophobic block. The pyridine moiety brings unique coordination ability and environmental responsiveness, enabling interactions with a broad range of metal ions and pH-dependent changes in polymer behaviour. Such features are highly attractive for developing catalytic, sensing, or stimuli-responsive stomatocyte systems. However, even subtle changes in the hydrophobic block of PEG-PS copolymers are known to strongly affect self-assembly and shape transformation. Therefore, understanding how 4VP content and placement influence polymersome formation and stomatocyte yield is essential for leveraging this functional monomer without compromising morphological control. This prompted us to construct PEG-*b*-P(S-*co*-4VP) copolymers and to study their assembly and shape change into stomatocytes. This work systematically investigates these effects, providing the mechanistic insight needed to design functionalized stomatocytes with enhanced capabilities.

2. Results and discussion

2.1 Block copolymer design

To explore the impact of 4-vinylpyridine (4VP) incorporation on both the self-assembly and shape transformation of poly (ethylene glycol)-*block*-polystyrene (PEG-PS) block copolymers, we synthesized a series of amphiphilic block copolymers in which the molar fraction of 4VP and its position in the hydrophobic block were varied using reversible addition–fragmentation chain-transfer (RAFT) polymerization. This method enabled precise control over the polymerization process, resulting in polymers with low dispersity ($Đ \approx 1.1$) (Table 1 and Fig. S1–S7). We first designed a series of block copolymers in which the hydrophobic block consisted of a statistical copolymer of styrene and 4-vinylpyridine (4VP), with the molar ratio of 4VP systematically varied. To confirm that the hydrophobic block was indeed a statistical copolymer, we first determined the monomer reactivity ratios (r_{4VP} for 4VP and r_{St} for styrene) and used these to determine the intramolecular composition drift during the polymerization.[48] Low-conversion (<10%) copolymerizations with initial monomer mixtures containing different mole fractions of 4VP (f_{4VP} = 0.1, 0.2, 0.3, 0.5, 0.7, 0.8

Table 1 Chemical composition of the synthesized block copolymers

	M_n [a] (kg mol^{-1})	$Đ$[b]	DP-St[a]	DP-4VP[a]	f_{4VP}	f^*
P1: A–(B–C)/0.06 PEG-*b*-P(S160-*co*-4VP10)	20	1.09	160	10	0.06	0.26
P2: A–(B–C)/0.11 PEG-*b*-P(S155-*co*-4VP20)	21	1.07	155	20	0.11	0.25
P3: A–(B–C)/0.14 PEG-*b*-P(S190-*co*-4VP30)	26	1.11	190	30	0.14	0.20
P4: A–B–C/0.06 PEG-*b*-PS150-*b*-P4VP10	19	1.09	150	10	0.06	0.28
P5: A–C–B/0.09 PEG-*b*-P4VP15-*b*-PS150	20	1.10	150	15	0.09	0.27

[a] Number-average molecular weight and degree of polymerization were calculated from ^{1}H-NMR measurements. [b] Polydispersity measured by gel permeation chromatography (GPC). f_{4VP} = the mole fraction of 4VP within the hydrophobic block, calculated from ^{1}H-NMR measurements. f^* = hydrophilic-to-hydrophobic mole ratio. Polymers are denoted as A–(B–C)/x (where A = PEG, B = PS, C = P4VP, and x represents the mole fraction of 4VP within the hydrophobic block).

and 0.9) were carried out, and the (~instantaneous) copolymer compositions were determined by proton NMR spectroscopy (Fig. S8 and S9). Reactivity ratios of $r_{4VP} = 0.5$ and $r_{St} = 1.2$ were estimated from these data using the Fineman–Ross and Kelen–Tüdös procedures (Fig. S10) and subsequently used to determine the intramolecular composition drift (Fig. S11). For both the polymers with the lowest ($f_{4VP} = 0.06$) and highest ($f_{4VP} = 0.14$) amounts of 4VP, we observed a relatively constant instantaneous copolymer composition up to high conversion (which is indicative of a completely statistical incorporation of the comonomers), with a final small drift that indicated that the terminal parts of the chains are short 4VP segments. Hence, it is safe to conclude that RAFT polymerization of styrene and 4VP under our polymerization conditions leads to statistical copolymer compositions and not to blocky or (real) gradient copolymers.

We subsequently synthesized three statistical amphiphilic block copolymers using a poly(ethylene glycol) (PEG)-based macro-RAFT agent with different 4VP molar ratios by simultaneously adding styrene and 4VP at the start of the polymerization (Scheme 1). These polymers, denoted as A–(B–C)/x (where A = PEG, B = PS, C = P4VP, and x represents the mole fraction of 4VP within the hydrophobic block), are detailed in Table 1. To further investigate the effect of block arrangement, we synthesized two additional tri-block copolymers with distinct architectures: A–B–C (PEG-*b*-PS-*b*-P4VP) and A–C–B (PEG-*b*-P4VP-*b*-PS). For the A–B–C copolymer, styrene was polymerized first, followed by 4VP after complete styrene polymerization. Conversely, for the A–C–B copolymer, 4VP was polymerized first, followed by styrene (Table 1).

2.2 Morphological properties of polymeric vesicles

Spherical polymeric vesicles were prepared using the solvent-switch method. In this approach, the polymer was first dissolved in a good solvent for both blocks, followed by the addition of a non-solvent for the hydrophobic block to induce self-assembly. We used a tetrahydrofuran (THF)–dioxane mixture as the good solvent and added water to trigger self-assembly. Thereafter, the organic solvent was removed *via* dialysis (against either 10 mM or 20 mM NaCl solution), inducing shape transformation of the formed polymersomes. Dynamic light scattering (DLS) and electron microscopy (EM) measurements were performed to characterize the hydrodynamic size and topology, respectively, of the polymeric vesicles. Moreover, we employed asymmetric flow field-flow fractionation (AF4) coupled with multi-angle light scattering (MALS) and quasi-elastic light scattering (QELS) detectors to quantitatively analyse the results of the shape transformation processes. This setup allows simultaneous measurement of both the radius of gyration (R_g) and the hydrodynamic radius (R_h). The

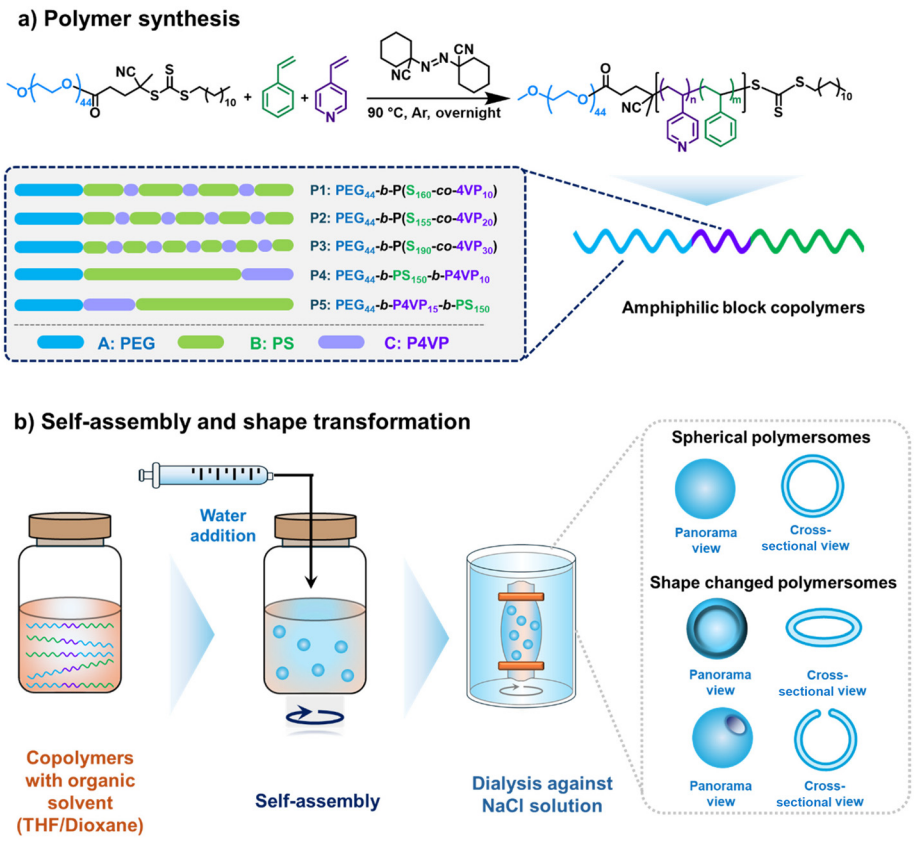

Scheme 1 (a) PEG_{44}-*b*-P(S_m-*co*-$4VP_n$) polymer synthesis and overview of the synthesized copolymers. (b) General scheme of the self-assembly and shape transformation process.

ratio of R_g to R_h, known as the shape factor (ρ), provides valuable information about particle morphology. It is known that empty spheres have a ρ of 1, whereas filled spheres (hard spheres) have a ρ of 0.77.[49] Indeed, the spherical polymersomes showed a shape factor close to 1,[32] matching our expectations. Based on prior work on PEG-PS copolymer assemblies, it was shown that stomatocytes have a ρ between 0.8 and 0.9.[27] To this end, we set a shape factor threshold of 0.91 to distinguish stomatocytes from other morphologies, such as spheres, prolates or discs, all of which have a ρ of 1 or higher.[49,50] With this methodology, we first quantitatively analysed the shape transformation of PEG_{44}-*b*-PS_{185} polymersomes, which produced 77%, 74% and 82% stomatocytes upon dialysis against 10 mM, 20 mM, and 35 mM NaCl, respectively (Fig. S12), confirming the reliability of our approach. This 4VP-free control confirms that the dialysis conditions do not significantly affect the stomatocyte population.

We subsequently investigated the effect of random incorporation of different mole fractions of 4VP (*i.e.*, 0.06, 0.11 and 0.14, P1–P3 respectively). All three polymers successfully self-assembled into vesicular structures, as observed by scanning electron microscopy (SEM) and transmission electron microscopy (TEM) (Fig. S13–S16). When dialyzed against a 10 mM NaCl solution, polymers P1–P3 yielded mixed populations of spherical vesicles and stomatocytes (Fig. S13–S16) as observed by both SEM and TEM. Complementary AF4-QELS and DLS analyses further indicated that P1 and P2 generated smaller structures compared to P3 (Fig. S17), consistent with the microscopy observations. AF4-MALS-QELS shape-factor analysis also revealed a minor population of stomatocytes in P2 (4%, Fig. S13c), which was even lower compared to the populations obtained from P1 (18%) and P3 (27%) (Fig. S13c). In all three cases, the amount of stomatocytes formed was significantly lower compared to the regular PEG-PS samples (*i.e.*, the control polymer without 4VP), indicating that minimal incorporation of 4VP negatively impacts the efficiency of shape transformation into stomatocytes.

As dialysis against higher salt concentrations is known to facilitate shape transformation to stomatocytes, we employed 20 mM NaCl during dialysis. Indeed, we noticed a stronger tendency for stomatocyte structures to form, as shown in SEM and TEM images (Fig. 1a, b and Fig. S14–16). This trend was especially clear in polymers with higher 4VP content (P2 and P3) in which the stomatocyte populations increased to 36% and 52%, respectively. These findings suggest that although 4VP incorporation influences shape transformation, appropriate adjustment of dialysis conditions can yield samples enriched in stomatocytes. Consistent with the 10 mM dialysis results, DLS and AF4-QELS analyses indicated that P1 and P2 formed structures of comparable size (~200 nm), whereas P3 generated slightly larger assemblies with an average diameter of ~280 nm (Fig. 1d and Fig. S17).

To investigate how the polymer architecture influences self-assembly, we compared the self-assembly of polymers P1 (A–

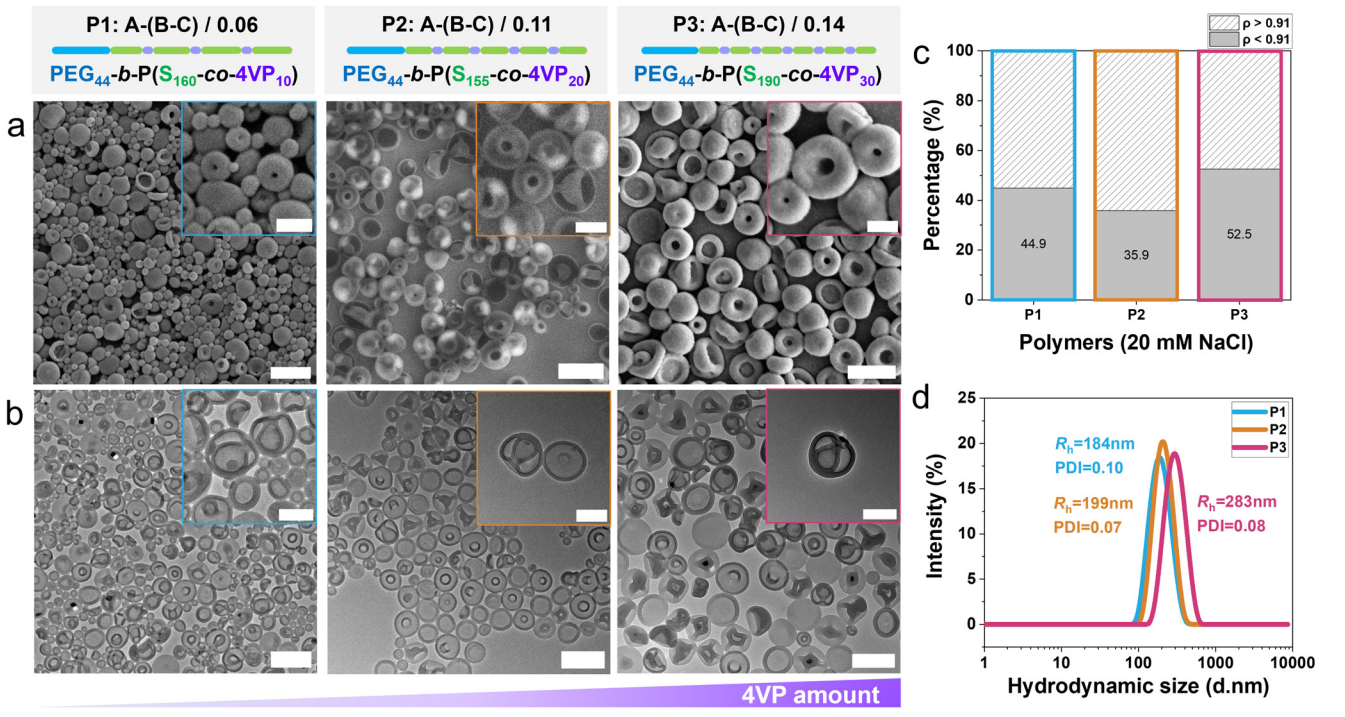

Fig. 1 The effect of 4VP content in statistical block copolymers on polymersome formation and shape transformation upon dialysis against 20 mM NaCl. (a) SEM and (b) TEM images of the samples. (c) Distribution analysis of polymeric vesicles calculated from AF4 data, displaying the percentage of stomatocytes. (d) Dynamic light scattering size–intensity comparison, displaying hydrodynamic diameter and PDI. EM scale bar = 500 nm, inset scale bar = 200 nm.

(B–C)/0.06), P4 (A–B–C/0.06), and P5 (A–C–B/0.09), each with similar hydrophilic-to-hydrophobic ratios (f = 0.26–0.28) and polystyrene (PS) mole fractions (f_{PS} = 0.72–0.75). After self-assembly, the organic solvent was removed *via* dialysis against 10 mM or 20 mM NaCl aqueous solutions, with representative electron microscopy images presented in Fig. S18 and S19. All samples had an average hydrodynamic size of approximately 200 nm, as measured by DLS and AF4-QELS (Fig. S20). TEM images and AF4-MALS-QELS analysis of samples prepared with 10 mM dialysis (Fig. 2a and b) revealed that polymer P4 (A–B–C/0.06), with 4VP at the chain end, produced a notably higher number of stomatocytes (43%), suggesting that shape transformation is less hindered in this polymer configuration. In contrast, when 4VP was in the middle (P5: A–C–B/0.09), fewer stomatocyte structures were formed (12%). For all three polymers, dialysis at 20 mM NaCl resulted in a clear increase in polymersome stomatocyte content (Fig. 2c and d; 45%, 53% and 55% for P1, P4 and P5, respectively), consistent with our findings for the statistical copolymer samples. Moreover, samples obtained by dialysis against 20 mM NaCl exhibited more uniform neck sizes –the openings connecting the inner lumen to the external environment – as observed in the inset images of Fig. 1b and 2c. However, sample heterogeneity limited the ability to draw definitive conclusions regarding neck dimensions. AF4-MALS-QELS analysis further revealed that the increase in stomatocyte formation was less pronounced for the A–B–C (PEG-*b*-PS-*b*-P4VP) system, suggesting that when 4VP is positioned at the chain terminus, its assembly more closely resembles that of PEG-PS-based stomatocytes, where stomatocyte formation is less sensitive to dialysis salt concentration (Fig. S12).

To assess whether the placement of 4VP within the hydrophobic block influences self-assembly, we prepared both statistical and block-like architectures while also varying the 4VP content. No significant differences in assembly or shape transformation were observed between these architectures. This outcome is likely explained by the dominant influence of the polystyrene domain: the amorphous, chain-stiffening nature of the PS block, combined with its substantially higher degree of polymerization relative to 4VP. In contrast, P4VP contributes only a small fraction of the hydrophobic mass and remains partially masked within the PS-rich matrix.

Since the increase in salt concentration in the dialysis medium led to a higher population of stomatocytes, we studied this effect in more detail using samples made of polymer P1 by dialyzing them against Milli-Q water (no salt) and 10 mM, 15 mM, 20 mM, 35 mM and 50 mM NaCl solutions. Under all conditions, polymeric vesicles were effectively formed (Fig. 3 and Fig. S21). DLS measurements revealed that vesicles dialyzed against Milli-Q water exhibited slightly larger hydrodynamic sizes (238 nm) compared to those dialyzed against NaCl solutions (<200 nm) (Fig. 3a and b). This is expected due to the osmotic pressure induced by salt, which causes vesicle volume reduction and consequent shape transformations. Indeed, a further increase in salt concentration led to a significant increase in the stomatocyte population, up

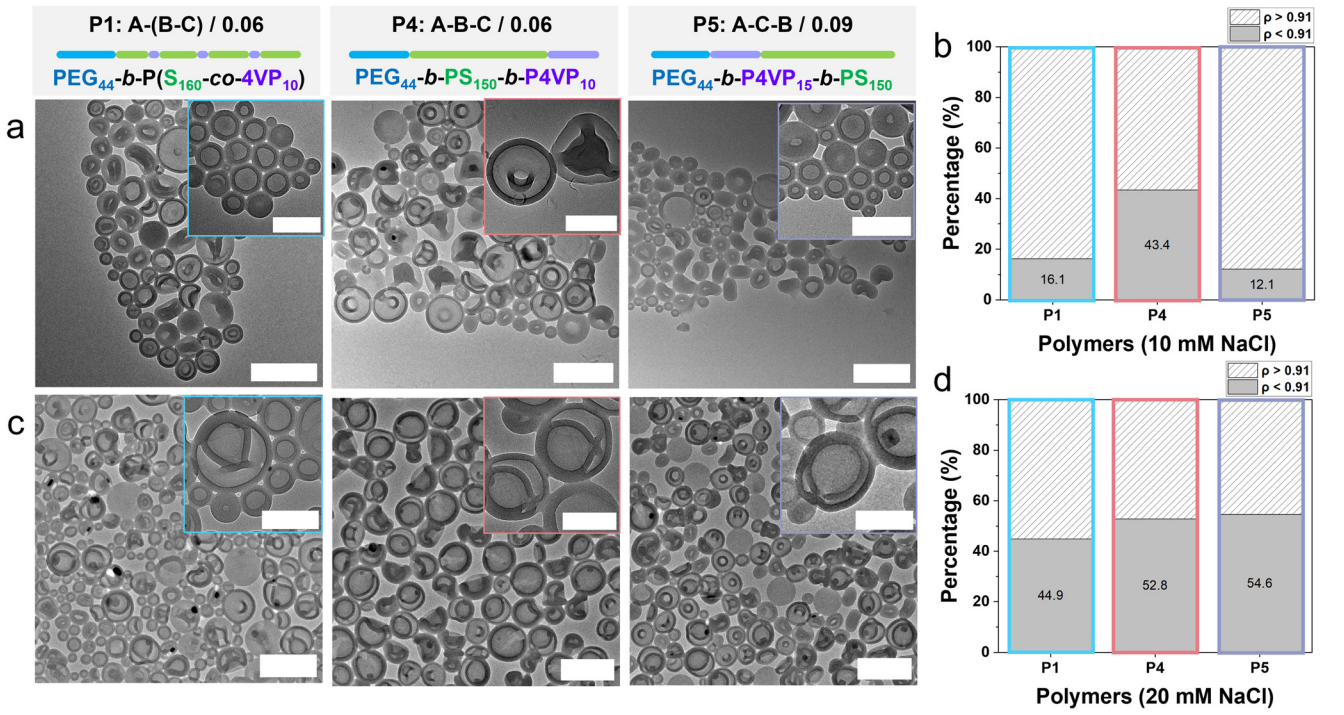

Fig. 2 The effect of block arrangement on polymersome formation and shape transformation. (a) TEM images of the samples dialyzed against 10 mM NaCl and (c) TEM images of the samples dialyzed against 20 mM NaCl. (b and d) Distribution analysis of polymeric vesicles calculated from AF4 data, displaying the percentage of stomatocytes. EM scale bar = 500 nm, inset scale bar = 200 nm.

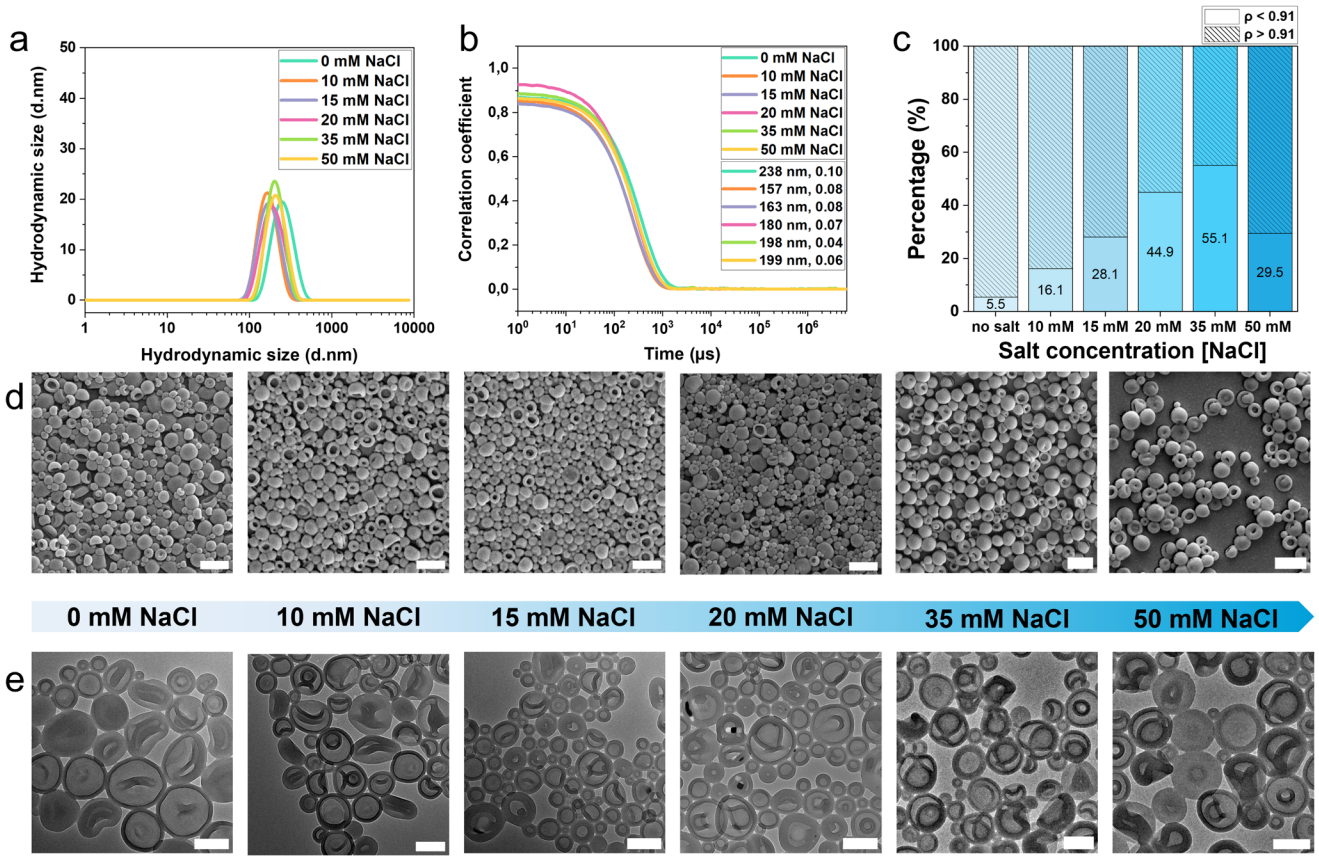

Fig. 3 Effect of NaCl concentration on the assembly of polymer P1: A–(B–C)/0.06 and the subsequent shape transformation. (a) Dynamic light scattering size–intensity comparison, (b) correlogram displaying hydrodynamic diameter and PDI, (c) distribution analysis of polymeric vesicles calculated from AF4 data, displaying the percentage of stomatocytes. (d) SEM and (e) TEM images of the samples prepared with different salt concentrations. SEM scale bar = 500 nm, TEM scale bar = 200 nm.

to 55% in 35 mM NaCl (Fig. 3c). We systematically examined the salt-dependent self-assembly and shape transformation of the PEG-PS-P4VP copolymers across a wide range of NaCl concentrations to further elucidate the contribution of the P4VP block. These experiments revealed that the presence of 4VP enhances the sensitivity of the vesicle-to-stomatocyte transition to ionic strength, in contrast to the more salt-robust behaviour of PEG-PS. Because this trend directly reflects how the additional block modulates membrane flexibility and solvent outflow during dialysis, we have emphasized its importance for understanding the functional influence of the P4VP segment.

Dialysis at a higher salt concentration (50 mM NaCl) yielded a reduced proportion of stomatocytes (30%, Fig. 3c), underscoring the critical influence of ionic strength on the morphology of PEG-PS-P4VP copolymers. At moderate NaCl levels, stomatocyte formation is favoured; however, beyond a threshold, control over shape transformation diminishes. This can be explained by the intricate interplay between shape change and particle vitrification. During self-assembly, the final solution contains ~50% organic solvent (THF–dioxane) after water addition, at which stage the amphiphilic polymer chains remain flexible. Subsequent dialysis removes the organic solvent trapped within the vesicles. Because the solvent outflow is not fully compensated by water influx, osmotic pressure develops, driving the vesicle-to-stomatocyte transformation. The rate of solvent removal, and thus the extent of shape change, is strongly modulated by the dialysis salt concentration. Once the organic solvent is expelled, the hydrophobic domains vitrify, locking in the resulting morphology. At elevated NaCl concentrations, the balance between osmotic pressure and solvent outflow is affected, and the shape transformation is quenched before complete stomatocyte formation. In the PEG-PS-P4VP system, 50 mM NaCl therefore proved too high, reducing the stomatocyte population. In contrast, vesicles formed from PEG_{44}-*b*-PS_{185} were comparatively insensitive to salt concentration; stomatocyte yields reached 74% at 20 mM NaCl and 82% at 35 mM, notably higher than the 55% stomatocytes observed for PEG-PS-P4VP (A–B–C/0.06) at 35 mM NaCl (Fig. 3c and Fig. S13).

The addition of the 4VP thus affects shape transformation, which can be modulated by optimizing dialysis conditions. To evaluate whether 4VP incorporation also introduces pH responsiveness at the morphological level, we varied the pH values of the sample solutions and observed no significant changes in size or morphology for any of the polymers, includ-

ing those containing 10 or 30 4VP units as well as the control without 4VP (Fig. S22). Within the investigated pH window (2–12), the control polymer PEG_{44}-*b*-PS_{185} exhibited a nearly constant average hydrodynamic diameter of ~300 nm. In the same range, polymer P3, containing 30 units of 4VP (f_{4VP} = 0.14; the highest 4VP fraction among the synthesized polymers), showed only minor variations in average hydrodynamic diameter (245–284 nm), which were not statistically significant. Likewise, vesicles prepared from P1 (statistical) and P4 (block), each containing 10 units of 4VP, exhibited essentially unchanged average hydrodynamic diameters of ~170–183 nm across pH 2–12 as well as the other polymers P2 (169–178 nm) and P5 (198–224 nm). Furthermore, TEM analysis confirmed that stomatocyte structures formed from PEG_{44}-*b*-P(S_{190}-*co*-$4VP_{30}$) remained intact at pH 2, pH 4.5, pH 6.9, and pH 12, indicating that the stomatocyte morphology is preserved across the tested pH range (Fig. S23). This insensitivity to pH is likely explained by the rigidity of the polystyrene domain, which restricts the extent to which the pH-responsive pyridine units can affect the overall morphology.

A wide variety of nanoreactors, defined as confined nanoscale reaction spaces, have been developed for diverse applications, where they offer protection of reactive species, spatial confinement, and enhanced selectivity/sensitivity.[51–53] Polymeric vesicles are particularly attractive nanoreactor platforms because they provide well-defined, hydrophobic compartments within aqueous media, enabling efficient reactions in a segregated environment.[54,55] Since 4VP is well known for its ability to coordinate metal ions, we demonstrate the potential of our new amphiphilic copolymer PEG–PS–P4VP as a versatile building block for metal-binding polymersome-based nanoreactors. First, we coordinated Cu(I) ions to the P4VP-containing stomatocytes and confirmed that the resulting Cu-loaded nanoreactors catalyze a model CuAAC reaction (Fig. 4), yielding a clear increase in fluorescence intensity compared to controls (*i.e.*, the free stomatocyte control (referred to as F-Sto; no copper treatment) and the reactants-only mixture (no vesicles)) (Fig. 4f). Importantly, TEM analysis showed that copper coordination did not alter the stomatocyte morphology, confirming that the functionalization is compatible with the structural integrity of the

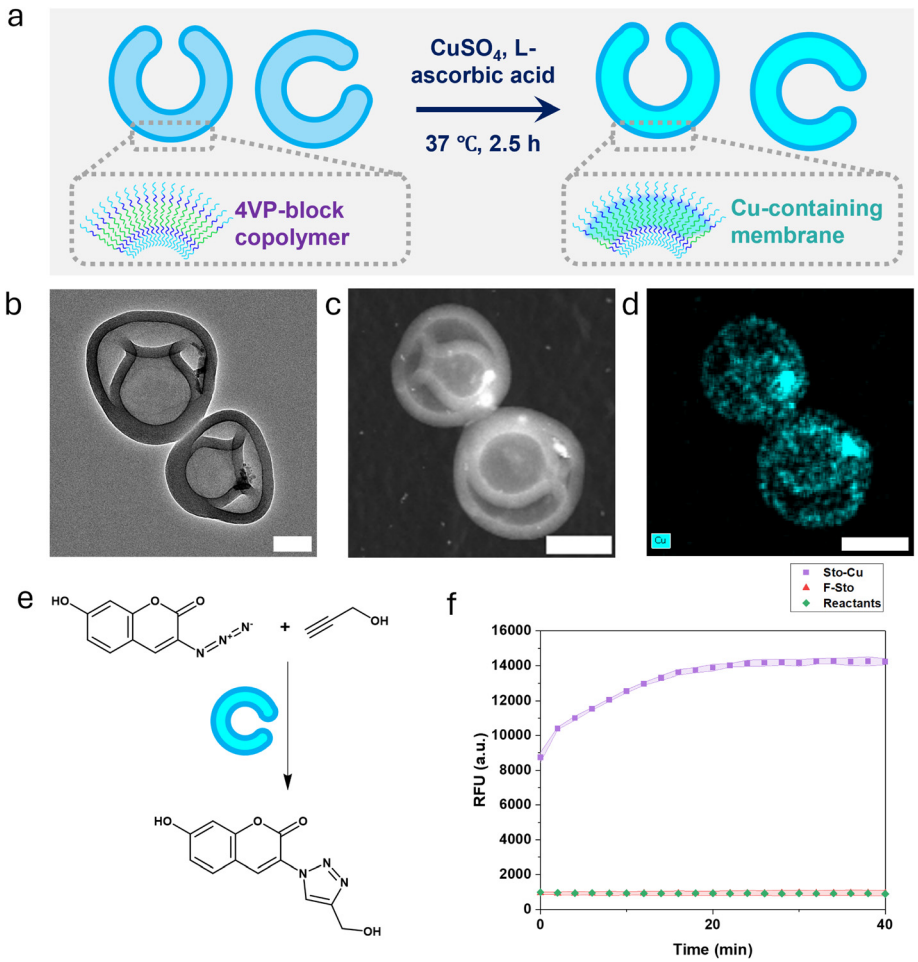

Fig. 4 (a) Schematic representation of copper nanoreactor preparation. (b) TEM image, (c) HAADF image and (d) TEM-EDX analysis of the stomatocytes after copper loading. (e) The CuAAC reaction between azido-coumarin and propargyl alcohol leads to a final product that is highly fluorescent. (f) Fluorescence intensity profile over 40 minutes of reaction time. Data are represented as mean ± SD n = 3 technical replicates. TEM scale bar = 100 nm.

assemblies (Fig. 4b), and copper was detected mostly on the membrane (Fig. 4d), where 4VP is present.

3. Conclusions

The self-assembly of PEG_{44}-*b*-P(S_m-*co*-$4VP_n$) block copolymers and their subsequent shape change in stomatocytes were studied, and the effect of 4VP addition to the amphiphilic polymer was systematically investigated (i) by varying the 4VP content, (ii) by changing the randomness of the block copolymers and (iii) by changing the dialysis conditions. It is worth noting that the addition of the third monomer even in small portions compared to polystyrene affects the self-assembly and shape transformation. With this work, we provide an insight into supramolecular architectures and how to achieve greater control over stomatocyte structures using a functional polymer. We found that the insertion of 4-vinylpyridine into PEG-PS copolymers represents a hurdle during shape transformation. This can be overcome by higher concentrations of NaCl solutions in dialysis, especially when 4VP is used in higher contents and/or is placed in between the PEG and PS blocks. In our system, the polystyrene segment is substantially longer than the P4VP block and therefore dominates the packing of the hydrophobic domain during self-assembly. As a result, the membrane organization is effectively PS-driven, with the shorter P4VP segment contributing less to the structural arrangement and thus being unlikely to generate chemical asymmetry within the bilayer. Consistent with this interpretation, we observed no measurable differences in size, zeta potential, or morphology between statistical and block-like architectures. Upon optimization of the dialysis conditions, also for the 4VP containing polymersomes, the stomatocyte morphology can be effectively formed, which opens opportunities for the introduction of chemical functionality into the polymer membrane with this interesting morphology.

Conflicts of interest

The authors declare no conflict of interest.

Data availability

The data supporting this article have been included as part of the supplementary information (SI). Supplementary information is available. See DOI: https://doi.org/10.1039/d5py01163a.

Data are available upon request from the corresponding authors.

Acknowledgements

This work is part of the Advanced Research Center for Chemical Building Blocks, ARC CBBC, which is co-founded and co-financed by the Dutch Research Council (NWO) and the Netherlands Ministry of Economic Affairs and Climate Policy. This research is financially supported by the Dutch Ministry of Education, Culture and Science (Gravity Program 024.005.020 – Interactive Polymer Materials, IPM). Electron microscopy was performed at the Center for Multiscale Electron Microscopy, Department of Chemical Engineering and Chemistry, Eindhoven University of Technology. The authors acknowledge Dr Maarten Bransen for performing the TEM-EDX measurements.

References

1 C. K. Wong, X. Qiang, A. H. E. Müller and A. H. Gröschel, *Prog. Polym. Sci.*, 2020, **102**, 101211.
2 J. K. Kim, S. Y. Yang, Y. Lee and Y. Kim, *Prog. Polym. Sci.*, 2010, **35**, 1325–1349.
3 S. Förster and T. Plantenberg, *Angew. Chem., Int. Ed.*, 2002, **41**, 688–714.
4 A.-V. Ruzette and L. Leibler, *Nat. Mater.*, 2005, **4**, 19–31.
5 D. E. Discher and A. Eisenberg, *Science*, 2002, **297**, 967–973.
6 Y. Mai and A. Eisenberg, *Chem. Soc. Rev.*, 2012, **41**, 5969–5985.
7 S. J. Hunter and S. P. Armes, *Langmuir*, 2020, **36**, 15463–15484.
8 Y. Liu, F. Ke, Y. Li, Y. Shi, Z. Zhang and Y. Chen, *Nano Res.*, 2023, **16**, 564–582.
9 H. Liu, J. Gong, P. Cao, L. Yang, L. Tao, X. Pei, T. Wang, Q. Wang, J. Zhang and Y. Zhang, *ACS Appl. Polym. Mater.*, 2024, **6**, 4789–4797.
10 G. A. Husseini and W. G. Pitt, *Adv. Drug Delivery Rev.*, 2008, **60**, 1137–1152.
11 N. Nishiyama, Y. Bae, K. Miyata, S. Fukushima and K. Kataoka, *Drug Discovery Today:Technol.*, 2005, **2**, 21–26.
12 Y. Zheng, Y. Oz, Y. Gu, N. Ahamad, K. Shariati, J. Chevalier, D. Kapur and N. Annabi, *Nano Today*, 2024, **55**, 102147.
13 A. Choucair, C. Lavigueur and A. Eisenberg, *Langmuir*, 2004, **20**, 3894–3900.
14 I. A. B. Pijpers, F. Meng, J. C. M. Van Hest and L. K. E. A. Abdelmohsen, *Polym. Chem.*, 2020, **11**, 275–280.
15 A. Blanazs, S. P. Armes and A. J. Ryan, *Macromol. Rapid Commun.*, 2009, **30**, 267–277.
16 E. J. Cornel, J. Jiang, S. Chen and J. Du, *CCS Chem.*, 2021, **3**, 2104–2125.
17 M. P. Vena, D. De Moor, A. Ianiro, R. Tuinier and J. P. Patterson, *Soft Matter*, 2021, **17**, 1084–1090.
18 L. Zhang and A. Eisenberg, *Macromolecules*, 1999, **32**, 2239–2249.
19 Y. Yu, L. Zhang and A. Eisenberg, *Macromolecules*, 1998, **31**, 1144–1154.
20 M. Dionzou, A. Morère, C. Roux, B. Lonetti, J.-D. Marty, C. Mingotaud, P. Joseph, D. Goudounèche, B. Payré, M. Léonetti and A.-F. Mingotaud, *Soft Matter*, 2016, **12**, 2166–2176.
21 J. Du and R. K. O'Reilly, *Soft Matter*, 2009, **5**, 3544–3561.
22 Y. Liu, D. H. T. Le, G. Yilmaz, L. Paffen, S. Li, A. B. Cook, T. Patiño Padial, L. Abdelmohsen, C. R. Becer, B. Sun and

J. C. M. Van Hest, *ACS Appl. Mater. Interfaces*, 2025, **17**, 35230–35239.
23 A. D. Fusi, Y. Li, M. M. E. Tholen, M. Cieraad, L. Albertazzi, T. Patiño Padial, J. C. M. Van Hest and L. K. E. A. Abdelmohsen, *J. Mater. Chem. B*, 2024, **12**, 11389–11401.
24 I. A. B. Pijpers, S. Cao, A. Llopis-Lorente, J. Zhu, S. Song, R. R. M. Joosten, F. Meng, H. Friedrich, D. S. Williams, S. Sánchez, J. C. M. Van Hest and L. K. E. A. Abdelmohsen, *Nano Lett.*, 2020, **20**, 4472–4480.
25 Y. Guo, J. Wang, G. Li, Z. Wang, Y. Li, S. Sun, J. C. M. Van Hest, M. Shen and X. Shi, *Adv. Funct. Mater.*, 2025, **35**, 2500113.
26 J. Shao, S. Cao, H. Che, M. T. De Martino, H. Wu, L. K. E. A. Abdelmohsen and J. C. M. Van Hest, *J. Am. Chem. Soc.*, 2022, **144**, 11246–11252.
27 L. K. E. A. Abdelmohsen, M. Nijemeisland, G. M. Pawar, G.-J. A. Janssen, R. J. M. Nolte, J. C. M. Van Hest and D. A. Wilson, *ACS Nano*, 2016, **10**, 2652–2660.
28 J. Shao, S. Cao, H. Wu, L. K. E. A. Abdelmohsen and J. C. M. Van Hest, *Pharmaceutics*, 2021, **13**, 1833.
29 H. Che, L. N. J. De Windt, J. Zhu, I. A. B. Pijpers, A. F. Mason, L. K. E. A. Abdelmohsen and J. C. M. Van Hest, *Chem. Commun.*, 2020, **56**, 2127–2130.
30 K. T. Kim, J. Zhu, S. A. Meeuwissen, J. J. L. M. Cornelissen, D. J. Pochan, R. J. M. Nolte and J. C. M. Van Hest, *J. Am. Chem. Soc.*, 2010, **132**, 12522–12524.
31 L. K. E. A. Abdelmohsen, F. Peng, Y. Tu and D. A. Wilson, *J. Mater. Chem. B*, 2014, **2**, 2395–2408.
32 L. K. E. A. Abdelmohsen, R. S. M. Rikken, P. C. M. Christianen, J. C. M. Van Hest and D. A. Wilson, *Polymer*, 2016, **107**, 445–449.
33 R. S. M. Rikken, S. Kleuskens, L. K. E. A. Abdelmohsen, H. Engelkamp, R. J. M. Nolte, J. C. Maan, J. C. M. Van Hest, D. A. Wilson and P. C. M. Christianen, *Soft Matter*, 2024, **20**, 730–737.
34 M. Nijemeisland, L. K. E. A. Abdelmohsen, W. T. S. Huck, D. A. Wilson and J. C. M. Van Hest, *ACS Cent. Sci.*, 2016, **2**, 843–849.
35 M. C. M. Van Oers, F. P. J. T. Rutjes and J. C. M. Van Hest, *J. Am. Chem. Soc.*, 2013, **135**, 16308–16311.
36 J. Albadi, M. Keshavarz, F. Shirini and M. Vafaie-nezhad, *Catal. Commun.*, 2012, **27**, 17–20.
37 F. Wen, W. Zhang, G. Wei, Y. Wang, J. Zhang, M. Zhang and L. Shi, *Chem. Mater.*, 2008, **20**, 2144–2150.
38 E. Hobbollahi, M. List and U. Monkowius, *Monatsh. Chem.*, 2019, **150**, 877–883.
39 H. Nazarpour-Fard, F. Shirini and G. B. Pour, *Inorg. Chem. Commun.*, 2025, **172**, 113691.
40 M. Antonietti, E. Wenz, L. Bronstein and M. Seregina, *Adv. Mater.*, 1995, **7**, 1000–1005.
41 R. Liu, S. Wang, J. Yao, W. Xu and H. Li, *RSC Adv.*, 2014, **4**, 38234–38240.
42 W.-M. Wan and C.-Y. Pan, *Polym. Chem.*, 2010, **1**, 1475–1484.
43 Z. Song, X. He, C. Gao, H. Khan, P. Shi and W. Zhang, *Polym. Chem.*, 2015, **6**, 6563–6572.
44 C. Huang, J. Tan, Q. Xu, J. He, X. Li, D. Liu and L. Zhang, *RSC Adv.*, 2017, **7**, 46069–46081.
45 P. Guo, W. Guan, L. Liang and P. Yao, *J. Colloid Interface Sci.*, 2008, **323**, 229–234.
46 A. Khanal, Y. Inoue, M. Yada and K. Nakashima, *J. Am. Chem. Soc.*, 2007, **129**, 1534–1535.
47 C. Wu, X. Wang, L. Zhao, Y. Gao, R. Ma, Y. An and L. Shi, *Langmuir*, 2010, **26**, 18503–18507.
48 J. P. A. Heuts and B. Klumperman, *Eur. Polym. J.*, 2024, **215**, 113215.
49 O. Stauch, R. Schubert, G. Savin and W. Burchard, *Biomacromolecules*, 2002, **3**, 565–578.
50 G. Lespes and V. De Carsalade Du Pont, *J. Sep. Sci.*, 2022, **45**, 347–368.
51 A. Lu and R. K. O'Reilly, *Curr. Opin. Biotechnol.*, 2013, **24**, 639–645.
52 V. Rodionov, H. Gao, S. Scroggins, D. A. Unruh, A.-J. Avestro and J. M. J. Fréchet, *J. Am. Chem. Soc.*, 2010, **132**, 2570–2572.
53 S. A. Dergunov, A. T. Khabiyev, S. N. Shmakov, M. D. Kim, N. Ehterami, M. C. Weiss, V. B. Birman and E. Pinkhassik, *ACS Nano*, 2016, **10**, 11397–11406.
54 L.-C. Lee, J. Lu, M. Weck and C. W. Jones, *ACS Catal.*, 2016, **6**, 784–787.
55 W. Sombat, P. Authai, P. Padungros and V. P. Hoven, *ACS Appl. Polym. Mater.*, 2023, **5**, 7288–7297.